Estimation and Correction of Geolocation Errors of the CFOSAT Scatterometer Using Coastline Backscatter Coefficients

Kuo Zhang, Xiaolong Dong, *Senior Member, IEEE*, Di Zhu, *Member, IEEE*, and Risheng Yun, *Member, IEEE*

***Abstract*—The scatterometer onboard the China-France Oceanography Satellite (CFOSAT) is the first rotating fan beam scatterometer (CSCAT) in operation. It is used to measure the ocean surface wind fields over a large observation swath. Geolocation is an important part of the preprocessing of scatterometer data. The accuracy of geolocation has a large impact on the accuracy of wind field retrieval. It is necessary to estimate and analyze the geolocation processing of CSCAT. The challenge is understanding how to estimate the geolocation errors of CSCAT. In this study, the coastline inflection method is used to estimate the geolocation errors of CSCAT based on the distribution characteristics of the backscatter coefficients at both the ocean and the land. The coastline inflection points are obtained using the gradient changes of backscatter coefficients near the coastline. The locations of these points are in line with the trend of the high-precision coastline data. The geolocation errors are estimated by comparing these points with the high-precision coastline. The results show that the current geolocation errors of CSCAT are about 7.31 km, which meets the requirements of 25 × 25 km wind field retrieval. In addition, because the geolocation of scatterometer data is affected by terrain, the geolocation errors of CSCAT are corrected based on an elevation correction algorithm using high-precision digital elevation model data. The results verify the effectiveness of the algorithm.**

***Index Terms*—Backscatter coefficients, coastline inflection method, geolocation errors, scatterometer.**

I. Introduction

THE spaceborne radar scatterometer is an active microwave remote sensor. When the scatterometer observes the ocean surface, its echo intensity is proportional to the amplitude of the scattering caused by the capillary gravity waves on the ocean surface, that is, the backscatter coefficient is positively related to the wind speed. The backscatter coefficient is also modulated by the wind direction, so the global ocean surface wind field can be retrieved using backscatter coefficient measured by scatterometer. The scatterometers previously operated in the industry mainly include fixed fan beam scatterometers and rotating scanning pen beam scatterometers. The China-France Oceanography Satellite Scatterometer (CSCAT) is the first internationally operated rotating scanning fan beam scatterometer [1]. The CSCAT can observe in continuous azimuth and elevation. It has the characteristics of covering a large observation swath (> 1000 km) and having high resolution. The main operating parameters and satellite orbit parameters of CSCAT are listed in Table I. At present, CSCAT runs stably, and it can retrieve ocean surface wind field products covering a 25 × 25 km grid. The accuracy of the wind speed is ± 2 m/s (wind speed 4–24 m/s), and the accuracy of wind direction is ±20° (360° wind direction range).

Geolocation errors provide an important reference index for the data measured by a satellite-based microwave instrument. Large geolocation errors will affect the calibration and verification of satellite data and subsequent related retrieval work [2]. Poe [3] analyzed the Special Sensor Microwave/Imager data and found that the potential geolocation errors originated from the ephemeris and attitude of the aircraft. The errors were reduced to 7 km by using accurate ephemeris and attitude data. Wiebe [4] optimized the level 1 data of the Advanced Microwave Scanning Radiometer onboard the Earth Observation System. It reduced the geolocation errors to 425 m (89 GHz) and 1425 m (6 GHz).

For spaceborne measurement instruments, two methods are usually used to estimate geolocation errors [5], the image correlation method [6], and the coastline inflection method [7]. The image correlation method transforms the ground control points generated by high-precision satellite geolocation to reference points and converts them into reference data that have the same form as the measured data. The geolocation errors are then estimated by comparing the reference data with the measured data. Data near a coastline are usually selected for comparison. Khlopenkov [8] used uniform ground control point data covering a study area of 5700 × 4800 km^2 to successfully estimate the subpixel geolocation errors of an Advanced High-resolution Radiometer with a resolution of 1 km. Purdy [9] compared image data corresponding to a coastline with its known geographical location, and completed an analysis of WindSat positioning and pointing accuracy, finding them to be 5 km and 0.5°, respectively. However, the spatial resolution of spaceborne microwave instruments data is relatively low, making it difficult to estimate geolocation errors by comparing

Manuscript received September 13, 2020; revised October 27, 2020; accepted October 28, 2020. Date of publication November 2, 2020; date of current version January 6, 2021. *(Corresponding author: Kuo Zhang.)*

Kuo Zhang is with the Key Laboratory of Microwave Remote Sensing, National Space Science Center, Chinese Academy of Sciences, Beijing 100190, China, and also with the University of Chinese Academy of Sciences, Beijing 100049, China (e-mail: 1219872763@qq.com).

Xiaolong Dong, Di Zhu, and Risheng Yun are with the Key Laboratory of Microwave Remote Sensing, National Space Science Center, Chinese Academy of Sciences, Beijing 100190, China (e-mail: dongxiaolong@mirslab.cn; zhudi@mirslab.cn; yunrisheng@mirslab.cn).

This article has supplementary downloadable material available at https://ieeexplore.ieee.org, provided by the authors.

Digital Object Identifier 10.1109/JSTARS.2020.3035238

TABLE I
TECHNICAL SPECIFICATIONS OF CSCAT

Operating parameters	
Frequency	13.256 GHz
Polarization	HH/VV
Bandwidth	0.5 MHz
Pulse duration	1.35 ms
Pulse repetition rate	150 Hz
Antenna spinning rate	3.4 rpm
Orbit parameters	
Orbit semi-major axis	6891.98 km
Eccentricity	0.00123
Orbit inclination	97.53°
Perigee angle	90°
Local time of descending intersection	7:00 AM
Orbital period	94.90 min

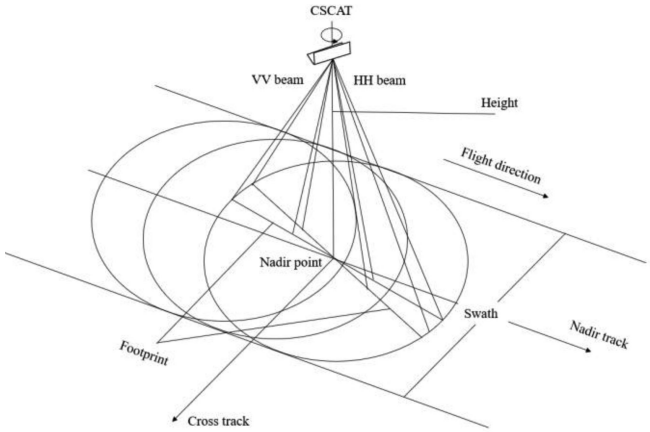

Fig. 1. Scan geometry of CSCAT.

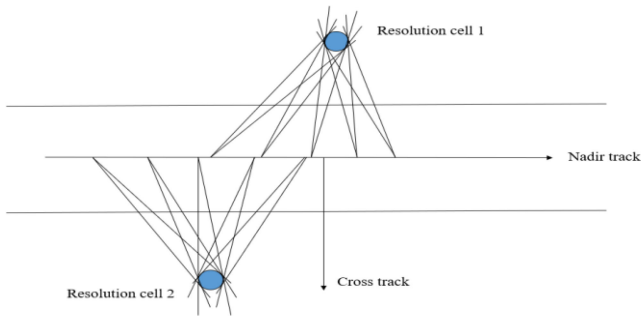

Fig. 2. Multiple observations of a resolution cell of CSCAT.

reference data of satellite imagery with measured satellite-based data. The coastline inflection method requires significant gradients in the data near the coastline, while the data acquired from a spaceborne microwave instrument meet this condition exactly [10]. This method is often used to estimate geolocation errors of microwave radiometers. For example, the Earth Radiation Budget Experiment scanner on the Earth Radiation Budget Satellite [7], the Atmospheric Infrared Sounder [11] on Aqua, the Cloud-Aerosol Lidar Infrared Pathfinder Satellite Observations [12], the Advanced Technology Microwave Sounder on the Suomi National Polar-orbiting Partnership [13], and the China FengYun-3C microwave radiation imager [5] all used this method. China launched the HY-2 satellite in 2011, and its rotating scanning pen beam microwave scatterometer also used this method to estimate the geolocation errors [10]. In this study, the coastline inflection method is used to estimate the geolocation errors of CSCAT.

The rest of this article is organized as follows. Section II briefly describes the scan geometry and geolocation algorithm of CSCAT. Section III describes the coastline inflection method and uses it to estimate the geolocation errors of CSCAT. Section IV introduces the digital elevation model (DEM) correction algorithm and shows how the optimized geolocation results were produced. Section V provides relevant conclusions.

II. CSCAT SCAN GEOMETRY AND GEOLOCATION ALGORITHM

A. CSCAT Scan Geometry

The CSCAT orbits at an altitude of about 519 km. Its rotating scanning fan beam system features two $1.2 \times 0.4 \times 0.4$ m waveguide slot array antennas. The antennas scan along the axis of the satellite nadir at a rate of 3.4 revolutions per minute with beamwidths of 14.5° and 15°, corresponding to vertically polarized (V-pol) and horizontally polarized (H-pol) observations, respectively. The corresponding fan footprints on the ground are approximately 250 km. The effective elevation angle of the two beams is between 26° and 46°. With the rotation of the antenna, an observation swath determined by the incident angle of the outer edge of the beam is formed, which is about 1000 km wide. Fig. 1 shows the scan geometry of CSCAT.

As shown in Fig. 2, CSCAT can acquire two or more observations of the same resolution cell as the satellite moves and the antenna rotates. The backscatter coefficient obtained through these measurements can be used to invert the ocean surface wind speed and direction. The microwave scatterometer needs to measure multiple azimuth angles on the same resolution cell and obtain the ocean surface wind vector through the model retrieval. Both the accuracy of ocean surface wind field retrieval and the possible fuzzy solutions in wind direction retrieval depend on the number of observations of the azimuth angles. When compared with the fixed fan beam scatterometer (the number of observations of the azimuth angles depends on the number of antennas) and the pencil beam scatterometer (the number of observations of the azimuth angles depends on the number of beams, with two single beam or four dual beams), the number of observations of the azimuth angles of CSCAT have greatly increased. The number of observations can reach more than ten in most areas within a swath, so its wind direction retrieval accuracy has greatly increased. The number of multiazimuth observations of a resolution cell located at the outer edge of the swath and the inner edge of the swath will be less than the resolution cell that fell in between the two ranges, which can be compensated by multipolarization measurement.

B. CSCAT Geolocation Algorithm

The CSCAT transmits a Ku-band chirp pulse signal to the surface of the earth and receives the echo signal. The baseband

echo signal is obtained after frequency conversion and dechirp processing. The CSCAT performs frequency offset processing on the transmitted signal based on a frequency precompensation lookup table (LUT_PC) because the difference between the Doppler frequencies offset by the beam near-end and far-end of the fan beam scatterometer is about 300 kHz [14]. This process ensures that the baseband echo signal is near zero frequency. The Doppler frequency offset of the fan-beam rotating scanning scatterometer varies with azimuth, elevation, and latitude of the nadir point. The CSCAT accumulates sampling points based on the slice division lookup table (LUT_SD) in order to obtain a ground observation slice of approximately 10 km. The accumulation is performed to obtain echo observation signals corresponding to 40 slices. The LUT_SD is obtained based on the correspondence between the residual Doppler frequency after precompensation plus the slant distance frequency and the observed slant distance. The geolocation of CSCAT is based on satellite ephemeris and attitude information, which is then combined with the frequency correspondence relationship to calculate the latitude and longitude of the 40 slice centers in each echo pulse and the corresponding observation angle information such as the incident and azimuth angles.

To calculate latitude and longitude, the algorithm needs to define the observation vector (H / V) in the instrument coordinate system according to the elevation and azimuth angles of the beam, and then convert the observation vector into the body coordinate system based on the antenna installation matrix that is measured before launch; then, the observation vector is transformed from the body coordinate system to the orbit coordinate system according to the 3-D rotation matrix related to the satellite attitude. The matrix can be expressed using the following equation:

$$T_{\text{sat}\to\text{orb}} = \begin{bmatrix} \cos(\text{yaw}) & -\sin(\text{yaw}) & 0 \\ \sin(\text{yaw}) & \cos(\text{yaw}) & 0 \\ 0 & 0 & 1 \end{bmatrix} \times \begin{bmatrix} \cos(\text{pitch}) & 0 & \sin(\text{pitch}) \\ 0 & 1 & 0 \\ -\sin(\text{pitch}) & 0 & \cos(\text{pitch}) \end{bmatrix} \begin{bmatrix} 1 & 0 & 0 \\ 0 & \cos(\text{roll}) & -\sin(\text{roll}) \\ 0 & \sin(\text{roll}) & \cos(\text{roll}) \end{bmatrix} \tag{1}$$

where yaw, pitch, and roll are the yaw, pitch, and roll angles, respectively. Next, the method uses GPS ephemeris data to transform the observation vector from the orbit coordinate system to the Earth-Centered Earth-Fixed coordinate system (ECEF) using the following equation:

$$T_{\text{orb}\to\text{ecef}} = [x\ y\ z] \tag{2a}$$

$$z = -\frac{p}{|p|} \tag{2b}$$

$$y = z \times \frac{v}{|z \times v|} \tag{2c}$$

$$x = y \times z. \tag{2d}$$

where p is the GPS satellite position vector and v is the GPS satellite velocity vector. The coordinates of surface observation point are calculated based on the obtained observation vectors in the ECEF coordinate system. Fig.3 shows the geometric relationship diagram, where x is the surface observation point vector, r is the observation vector, and d is the distance from the satellite to the surface observation point. The effect of the eccentricity of the earth is removed using the following equations:

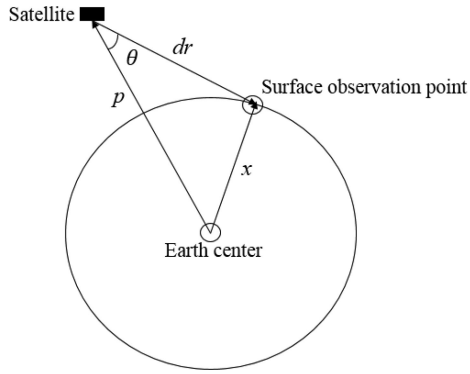

Fig. 3. Geometric relationship between the satellite, the earth center, and the surface observation point in the ECEF coordinate system.

$$r' = \left[\frac{r_1}{a}, \frac{r_2}{a}, \frac{r_3}{b}\right] \tag{3a}$$

$$p' = \left[\frac{p_1}{a}, \frac{p_2}{a}, \frac{p_3}{b}\right] \tag{3b}$$

$$x' = \left[\frac{x_1}{a}, \frac{x_2}{a}, \frac{x_3}{b}\right] \tag{3c}$$

where a is the semimajor axis of ellipsoid and b is the semiminor axis of ellipsoid. The distance from the satellite to the surface observation point is calculated based on cosine theorem and quantity product relationship ($|x'| = 1$):

$$|x'|^2 = |p'|^2 + |dr'|^2 - 2|p'||dr'|\cos(\theta) \tag{4a}$$

$$p' \cdot r' = -|p'||r'|\cos(\theta) \tag{4b}$$

$$d = \frac{-(p' \cdot r') - \sqrt{(p' \cdot r')^2 - \left(|p'|^2 - 1\right)|r'|^2}}{|r'|^2}. \tag{4c}$$

The coordinates of surface observation point can be expressed as follows:

$$x' = p' + dr' \tag{5a}$$

$$x = \left[\left(p_1' + dr_1'\right)a,\ \left(p_2' + dr_2'\right)a, \left(p_3' + dr_3'\right)b\right]. \tag{5b}$$

Finally, the surface observation point in the ECEF coordinate system is converted to the latitude and longitude in the geodetic coordinate system using the following equation:

$$\text{lon} = \tan^{-1}\left(\frac{x_2}{x_1}\right) \tag{6a}$$

$$\text{lat} = \tan^{-1}\left(\frac{\frac{x_3}{1-e^2}}{\sqrt{x_1^2 + x_2^2}}\right) \tag{6b}$$

where lon is the longitude, lat is the latitude, and e is the eccentricity of ellipsoid. The above is the basic geolocation algorithm of a microwave scatterometer. The elevation angles of the inner

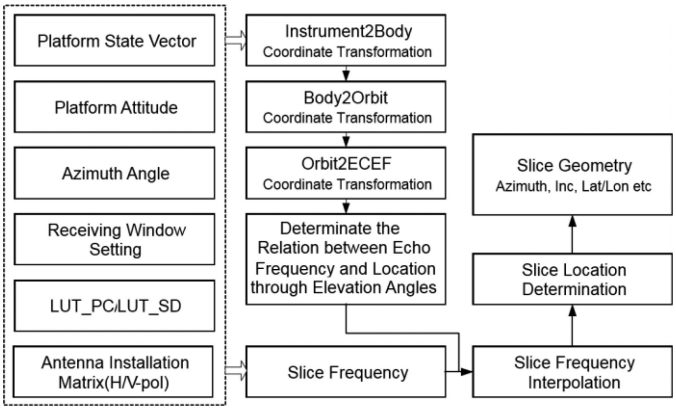

Fig. 4. Geolocation algorithm flow of CSCAT.

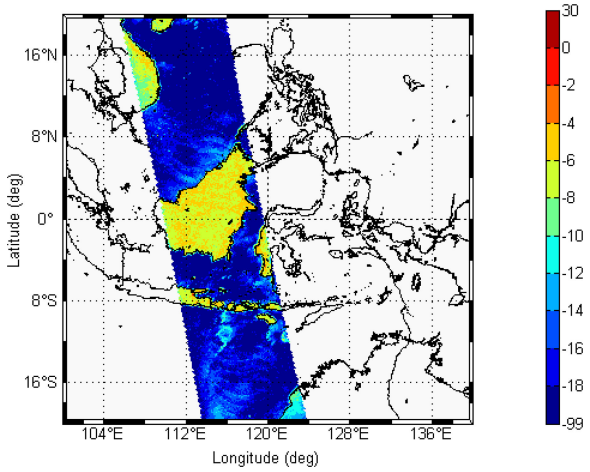

Fig. 5. Regional distribution of CSCAT backscatter, Indonesia, on the 2065th revolution on March 14, 2019.

and outer beams are fixed for the pencil beam scatterometer [15], so the geometric positioning of the observation point can be directly obtained by using the above algorithm. However, for the fan beam scatterometer [16], the elevation angles of the beam are in a dynamic range; for CSCAT the angle falls between 26° and 46°. If we need to achieve the geolocation of the fan beam scatterometer, it will be necessary to use the correspondence between the surface observation point and echo frequency based on the above algorithm. The echo frequency can be expressed as follows:

$$f_{\text{echo}} = f_{\text{slant}} + f_{\text{re}_{\text{doppler}}} \tag{7}$$

where f_{echo}, f_{slant} , and $f_{\text{re}_{\text{doppler}}}$ are the echo, slant, and the residual Doppler frequencies, respectively. The slant distance frequency is obtained by a dechirping processing on the signal [17] as follows:

$$f_{\text{slant}} = \frac{B\Delta t}{T_p} \tag{8}$$

where B is the signal bandwidth, T_p is the pulse width, and Δt is the signal delay. The residual Doppler frequency is the difference between the Doppler frequency of relative motion and the precompensation frequency:

$$f_{\text{re}_{\text{doppler}}} = \frac{2V_{\text{pro}}f_c}{c} - f_{\text{lut}_{\text{pc}}} \tag{9}$$

where V_{pro} is the projection of satellite velocity vector on the surface of the earth, c is the speed of light, f_c is the receiver carrier frequency, and $f_{\text{lut}_{\text{pc}}}$ is the precompensation frequency. Fig. 4 shows the flow pattern of the CSCAT geolocation algorithm.

III. CSCAT Estimation of Geolocation Errors

A. CSCAT Coastline Inflection Method

Using the coastline inflection method requires knowing the distribution characteristics of the backscatter from both the ocean and the land. Fig. 5 shows the backscatter of CSCAT L1B data passing through the ocean area near Indonesia; a significant change in gradient can be seen in the numerical values, indicating that the coastline inflection method can be used to estimate the CSCAT geolocation errors.

The method requires filtering the available data near the coastline during the estimation process. For CSCAT, when selecting data, the method finds the four slices closest to the coastline from the observation pulses as a group of measurements. However, each group of measured values must meet the relevant conditions before it can be used for geolocation error estimation. First, the backscatter coefficient value of each group must be increased or decreased appropriately; otherwise, the calculation of positioning reference points cannot be performed subsequently. Second, the difference between the maximum and minimum backscatter coefficient of each group must meet a certain threshold. This is done to ensure that the value chosen spans the values of land and ocean. Fig. 6 shows the range of the ocean and land backscatter coefficient values of CSCAT on March 14, 2019, the 2065th revolution. The red and blue points are land and ocean values, respectively. It can be seen that the backscatter coefficient values of the two can be clearly separated. The backscatter coefficient values on the ocean surface fluctuate widely because the ocean surface roughness varies with different wind speeds and directions. Compared with the ocean surface, the scattering on land is more stable and uniform. The statistical results show that the difference between the V-pol backscatter coefficient values of land and ocean is 5 dB, and the difference of H-pol is 6 dB. Therefore, the threshold of the backscatter coefficient values of each group was set to 6 dB. Because a large range of backscatter coefficients was observed on the ocean surface, after the above two conditions are met, it may happen that all backscatter coefficients fall on the ocean surface. The statistical results show that the group with backscatter coefficients values all lower than -14 dB is filtered out. In addition, backscatter may be affected by extreme weather (typhoons, heavy rain), which will cause the backscatter coefficient values on the ocean surface to be higher than normal, so this part of the data must also be removed.

A fine-resolution database known as the Global Self-consistent, Hierarchical, High-resolution Geography Database

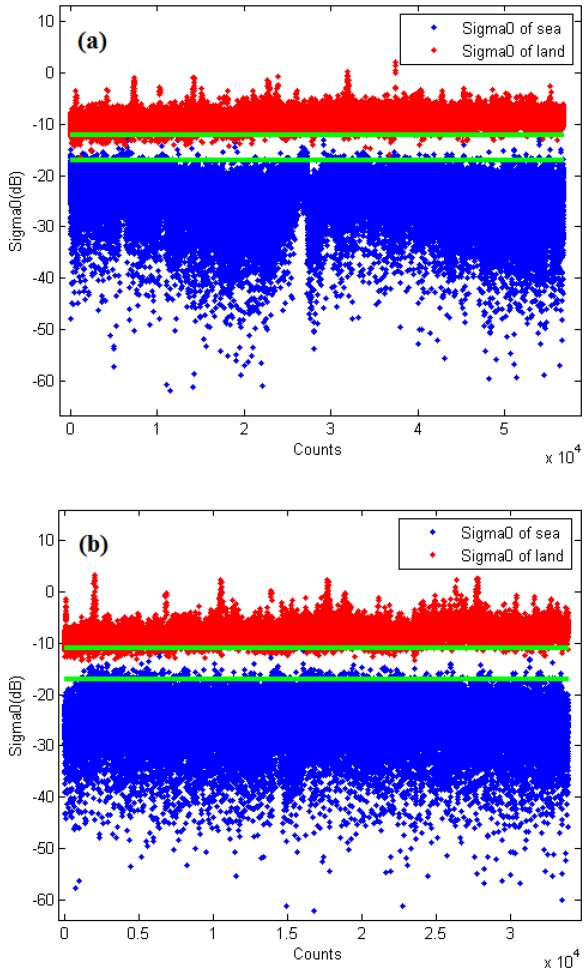

Fig. 6. Scatter plot of CSCAT ocean and land observations, on the 2065th revolution on March 14, 2019. (a) V-pol. (b) H-pol.

GSHHS [18] was used. The resolution of GSHHS (∼200 m) is quite high compared with CSCAT, so it is accurate enough to be used as reference data for estimation. The backscatter coefficient data from CSCAT, which passed through Hainan Island and Liaodong Bay, acquired from February 27 to April 10, 2019, were used. Fig. 7 shows the 2065th revolution data on March 14, 2019; all of the data were in the above time range. It can be seen that the backscatter coefficient values from the ocean to the land gradually increased over time.

The cubic function expression can be expressed as follows:

$$y_i = ax_i^3 + bx_i^2 + cx_i + d \tag{10}$$

where x_i is longitude or latitude of the group slice and y_i is backscatter coefficients value of the group slice. The function expression is based on selected revolutions. Each revolution can select some groups. The inflection point of each group is calculated by this function. Every group can fit a cubic curve (Fig. 8). The color of the rhombus dots in the figure transforms from yellow to blue, which indicates that the backscattering coefficient value decreases sequentially.

Coefficients of the function expression (a, b, c, d) are calculated using longitude or latitude and backscatter coefficient

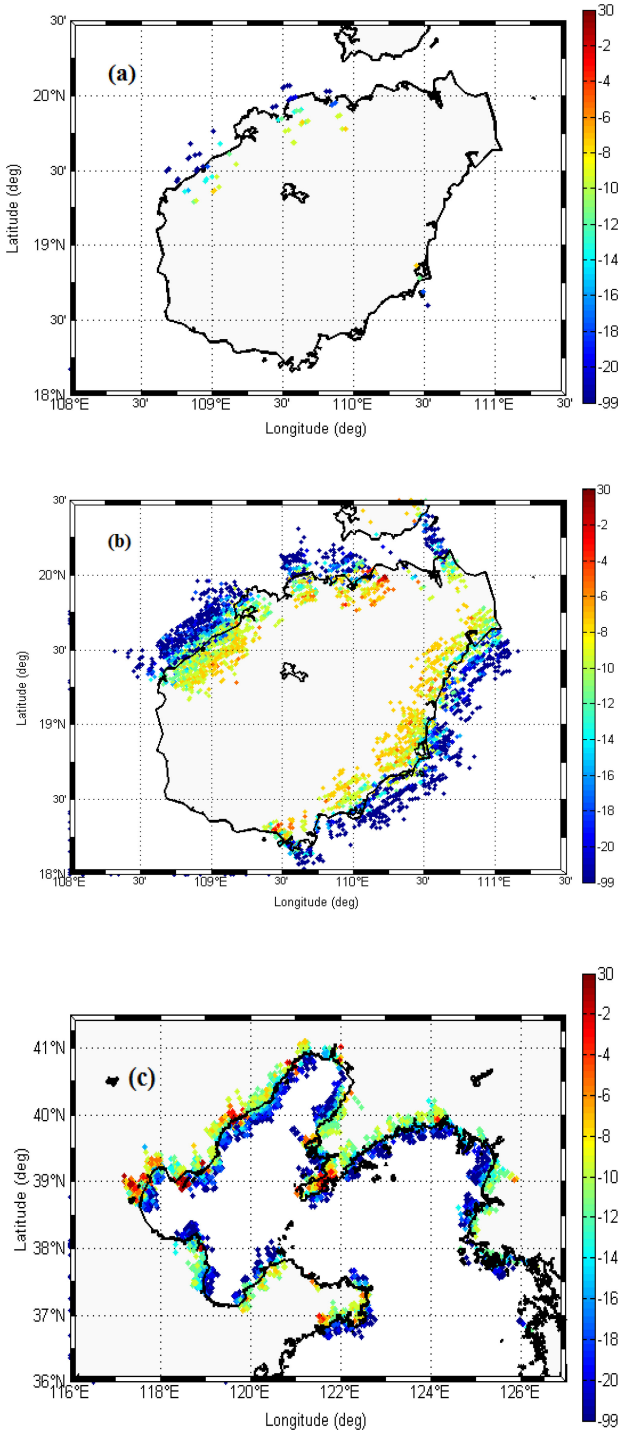

Fig. 7. Selection of a CSCAT group slice in Hainan Island and Liaodong Bay from February 27 to April 10, 2019: (a) The 2065th revolution over Hainan Island. (b) All revolutions over Hainan Island within the above time. (c) All revolutions over Liaodong Bay within the above time.

values of the group slice. The formula can be expressed as follows [7]:

$$\begin{bmatrix} a \\ b \\ c \\ d \end{bmatrix} = \begin{bmatrix} x_1^3 & x_1^2 x_1 & 1 \\ x_2^3 & x_2^2 x_2 & 1 \\ x_3^3 & x_3^2 x_3 & 1 \\ x_4^3 & x_4^2 x_4 & 1 \end{bmatrix}^{-1} \begin{bmatrix} y_1 \\ y_2 \\ y_3 \\ y_4 \end{bmatrix}. \tag{11}$$

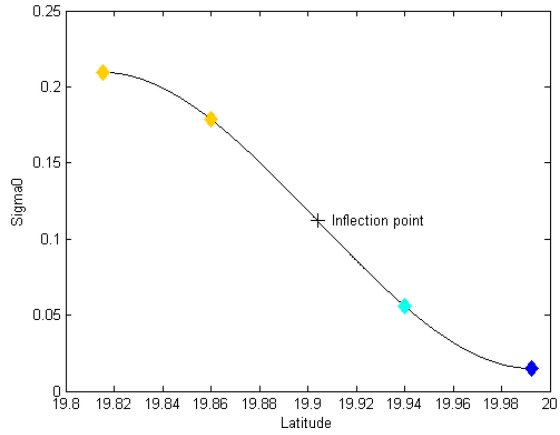

Fig. 8. Example of determining the inflection point using four slices closest to the coastline from the observation pulse along the latitude fit by a cubic function.

After finding the coefficients of the function, the second derivative of the function is equal to zero:

$$x = -b/3a \tag{12}$$

where x is the longitude or latitude of the inflection point of the group. The point of the plus sign in Fig. 8 is the calculated inflection point.

However, in the actual calculations, the calculated latitude and longitude of the inflection points of each group were affected by the randomness of the noise and the terrain, so that some calculated results are not between the latitudes and longitudes of the two inner slices. When the positions of the two inner slices are too close to each other, the calculated position of inflection point will fall outside a reasonable range. These groups were eliminated in the subsequent estimation and statistics of geolocation errors. Fig. 9 shows the distribution of Hainan Island and Liaodong Bay inflection points along the coastline. The reference coastline data are from the GSHHS high-precision database. It can be seen that the trend of inflection points obtained by the coastline inflection method is basically consistent with the high-precision coastline data.

B. CSCAT Geolocation Errors

After the intersection of the group slices line and the coastline was obtained, the distance between the intersection point and the inflection point was calculated and a statistical analysis is performed to obtain estimated geolocation errors. Because CSCAT is a dual-polarized rotating scanning system, the geolocation errors are based on the forward view (azimuth ranges are 0°–90° and 270°–360°) and the afterward view (azimuth range is 90°–270°), V-pol and H-pol, respectively. Fig. 10 shows the statistical results, where Total contains all observations, VVF is V-pol forward view, VVA is V-pol afterward view, HHF is H-pol forward view, and HHA is H-pol afterward view. The results show that the geolocation error distribution of the forward view and afterward view are different. The reason is that the error of the CSCAT antenna installation matrix coefficients causes a deviation of the azimuth angle. As a result, the forward and afterward views will vary.

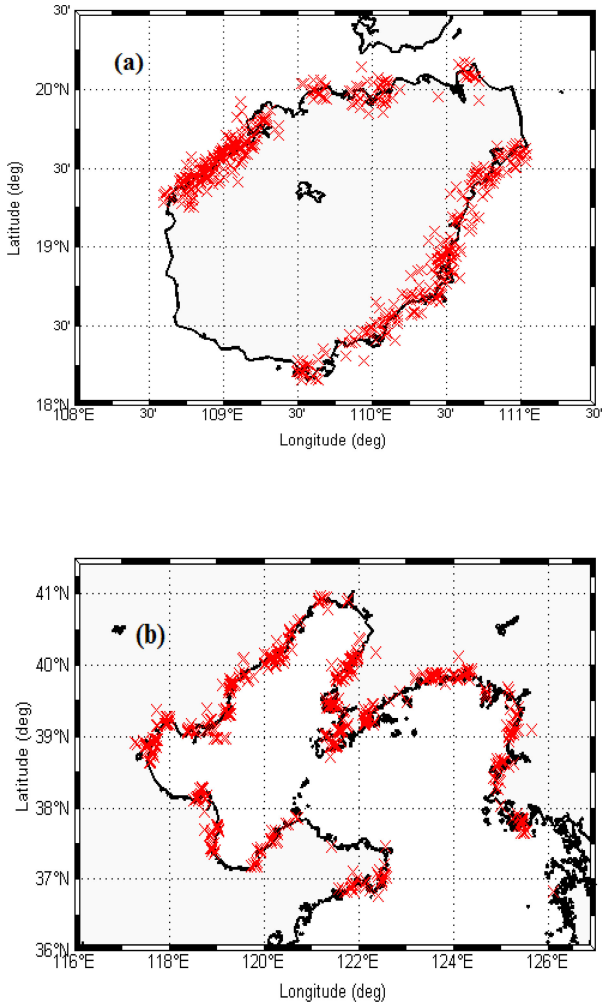

Fig. 9. Distribution of all inflection points from February 27 to April 10, 2019. (a) Hainan Island. (b) Liaodong Bay.

Table II shows the number of selected slice groups and the number of inflection points (eliminate incorrect points). It can be seen that the proportion of the number of selected slice groups in the inflection points of Total, VVF, VVA, HHF, and HHA are basically the same. Table III shows the geolocation errors of the four cases. The root mean square errors of all error values are calculated, and the currently estimated CSCAT geolocation errors is 7.31 km, which is less than half of the grid size of 25 × 25 km wind field products (<10 km) and meets the requirements of 25 × 25 km wind field retrieval.

IV. CSCAT Geolocation Error Corrections Based on the DEM Data

A. Correction Method

The changes in elevation across the terrain will also cause deviations in geolocation [19]. In Fig. 11, r is the observation vector in the ECEF coordinate system and x is the surface observation point on the reference ellipsoid. However, due to the influence of terrain, the backscatter coefficient measured is actually the value of the position of the intersection ($x^{'}$) between r and the

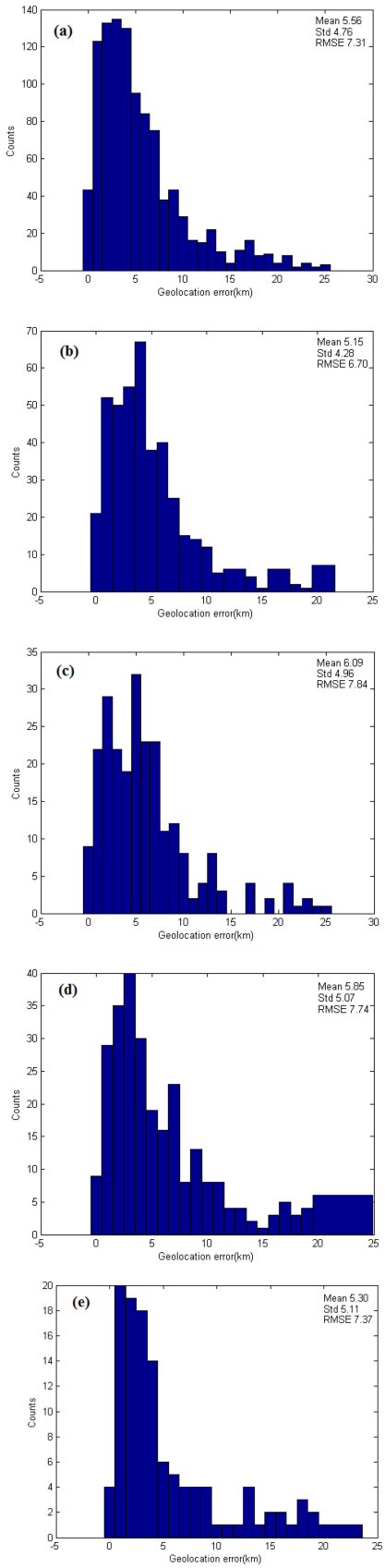

Fig. 10. Histogram distribution of geolocation errors from February 27 to April 10, 2019, including Hainan Island and Liaodong Bay. (a) Total. (b) VVF. (c) VVA. (d) HHF. (e) HHA.

TABLE II
NUMBER OF SELECTED SICE GROUPS, NUMBER OF INFLECTION POINTS, AND THEIR PERCENTAGES

	VVF	VVA	HHF	HHA	Total
Slice groups	596	328	378	160	1462
Inflection points	433	242	270	117	1062
Percentage	72.7%	73.8%	71.4%	73.1%	72.6%

TABLE III
GEOLOCATION ERRORS OF THE FOUR CASES

	VVF	VVA	HHF	HHA	Total
Geolocation errors(km)	6.70	7.84	7.74	7.37	7.31

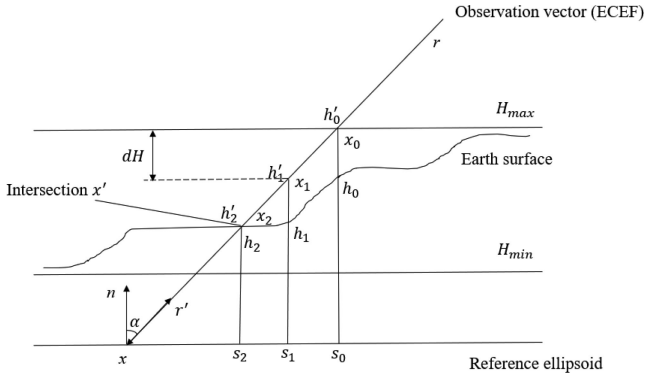

Fig. 11. Diagram of the DEM optimization algorithm.

earth surface instead of x. As a result, the calculated latitude and longitude do not match the backscatter coefficient, which causes geolocation deviation. Therefore, the DEM elevation data were used to optimize the geolocation algorithm.

The unit normal vector of the surface observation point can be expressed as (13):

$$n = [\cos(\text{lat})\cos(\text{lon}), \cos(\text{lat})\sin(\text{lon}), \sin(\text{lat})] \quad (13)$$

where lat and lon are the latitude and longitude of surface observation point. The unit observation vector and the angle between observation vector and the normal vector can be expressed as follows:

$$r' = -\frac{r}{|r|} \quad (14)$$

$$\cos\alpha = n \cdot r'. \quad (15)$$

The distance from the surface observation point to the maximum terrain height along the observation vector can be expressed as follows:

$$L_{\max} = \frac{H_{\max}}{\cos\alpha}. \quad (16)$$

The surface observation point vector corresponding to $L_{\max}$ can be expressed as follows:

$$x_0 = x + L_{\max} r'. \quad (17)$$

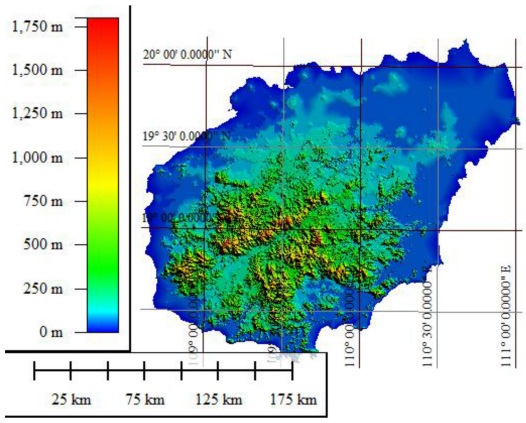

Fig. 12. DEM data with a resolution of 30 m covering the Hainan Island region.

In addition, the coordinates of the surface observation point s_0 can be obtained, which corresponds to x_0. The actual elevation value h_0 corresponds to s_0 based on the DEM data and h_0 is lower than h_0' ($H_{\max}$). The new surface observation point vector can be found by lowering the height as shown below:

$$h_1' = h_0' - dH \tag{18}$$

$$x_1 = x + \frac{h_1' r'}{\cos\alpha} \tag{19}$$

where h_1 is also lower than h_1'. The above process is then repeated until h is greater than or equal to h' ($h_2 \geq h_2'$). The surface observation point s_2 obtained at this time is the corrected surface observation point.

B. Correction Results

The Shuttle Radar Topography Mission provided high-precision elevation data [20] for the Hainan Island region, which was used to correct the geolocation errors. The spatial resolution of the Shuttle data is about 30 m, and the resolution of CSCAT is 25 km, which meets the requirements for calibration of CSCAT geolocation (0.03<<25 km). The data of Hainan Island region with elevation values above 200 m were selected to further reflect the effectiveness of the correction algorithm. Fig. 12 displays the DEM data of Hainan Island, which shows that the elevation gradually increases as the color changes from blue to red.

The level 1A data of CSCAT covering Hainan Island, corresponding to more than a month level 1B data used in Section III, were selected. The data were processed by the new geolocation algorithm, which was added to the above correction algorithm. The new level 1B data generated were used to compare the geolocation errors with the original level 1B data. Fig. 13 shows the statistical and comparison results before and after the geolocation optimization. The error distributions of the two are basically the same. The root mean square errors of the two situations were obtained. The geolocation errors before and after optimization were 6.89 and 5.83 km, respectively, so that the geolocation error was reduced by 1.06 km using DEM data.

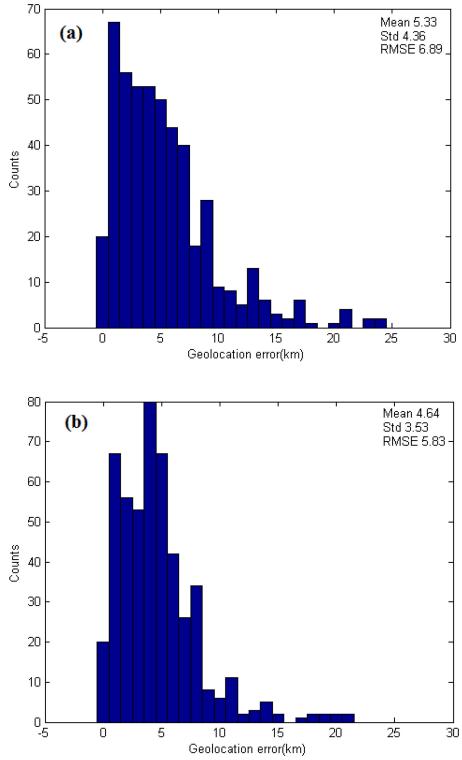

Fig. 13. Histogram distribution of geolocation errors: (a) Using the original data. (b) Using the optimized data correction by DEM optimization algorithm.

V. Conclusion

Based on the scan geometry and geolocation algorithm of CSCAT, this study used the coastline inflection method to estimate the geolocation errors of CSCAT. The GSHHS, a fine-resolution database, was selected. Hainan Island and Liaodong Bay in China were selected as the analysis areas. The geolocation errors were estimated using CSCAT L1B data collected from Hainan Island and Liaodong Bay from February 27 to April 10, 2019. A total of 1062 coastline inflection points were found that met the required conditions. The current geolocation errors of CSCAT were estimated to be approximately 7.31 km, which meets the conditions of 25 × 25 km wind field retrieval. In addition, high-precision DEM data were used to optimize the geolocation algorithm; the geolocation errors were reduced by about 1.06 km after optimization, which shows the effectiveness of this method for using an optimized geolocation algorithm. The CSCAT geolocation errors primarily come from satellite ephemeris and attitude errors, geolocation algorithm errors, and errors introduced by the rotation of the fan beam antenna. In the future, the causes of geolocation errors will be further analyzed and geolocation algorithms will be improved in order to further improve the accuracy of wind field retrieval for the rotating scanning fan beam microwave scatterometer and to obtain higher resolution wind field products.

References

[1] J. Liu *et al.*, "First results from the rotating fan beam scatterometer onboard CFOSAT," *IEEE Trans. Geosci. Remote Sens.*, to be published, doi: 10.1109/TGRS.2020.2990708.

[2] I. Moradi, H. Meng, R. R. Ferraro, and S. Bilanow, "Correcting geolocation errors for microwave instruments aboard NOAA satellites," *IEEE Trans. Geosci. Remote Sens.*, vol. 51, no. 6, pp. 3625–3637, Jun. 2013.
[3] G. A. Poe and R. W. Conway, "A study of the geolocation errors of the special sensormicrowave/Imager (SSM/I)," *IEEE Trans. Geosci. Remote Sens.*, vol. 28, no. 5, pp. 791–799, Sep. 1990.
[4] H. Wiebe, G. Heygster, and L. Meyer-Lerbs, "Geolocation of AMSR-E data," *IEEE Trans. Geosci. Remote Sens.*, vol. 46, no. 10, pp. 3098–3103, Oct. 2008.
[5] F. Tang, X. Zou, H. Yang, and F. Weng, "Estimation and correction of geolocation errors in FengYun-3C microwave radiation imager data," *IEEE Trans. Geosci. Remote Sens.*, vol. 54, no. 1, pp. 407–420, Jan. 2016.
[6] J. Le Moigne, N. S. Netanyahu, and R. D. Eastman, Eds., *Image Registration for Remote Sensing*. Cambridge, U.K.: Cambridge Univ. Press, 2011.
[7] L. H. Hoffman, W. L. Weaver, and J. F. Kibler, "Calculation and accuracy of ERBE scanner measurement locations," NASA Langley Res. Center, Hampton, VI, USA, Tech. Rep. NASA/TP-2670, 1987.
[8] K. V. Khlopenkov, A. P. Trishchenko, and Y. Luo, "Achieving subpixel georeferencing accuracy in the Canadian AVHRR processing system," *IEEE Trans. Geosci. Remote Sens.*, vol. 48, no. 4, pp. 2150–2161, Apr. 2010.
[9] W. E. Purdy, P. W. Gaiser, G. A. Poe, E. A. Uliana, T. Meissner, and F. J. Wentz, "Geolocation and pointing accuracy analysis for the WindSat sensor," *IEEE Trans. Geosci. Remote Sens.*, vol. 44, no. 3, pp. 496–505, Mar. 2006.
[10] Y. Zhang, M. Lin, and Q. Song, "Evaluation of geolocation errors of the Chinese HY-2A satellite microwave scatterometer," *IEEE Trans. Geosci. Remote Sens.*, vol. 56, no. 10, pp. 6124–6133, Oct. 2018.
[11] D. T. Gregorich and H. H. Aumann, "Verification of AIRS boresight accuracy using coastline detection," *IEEE Trans. Geosci. Remote Sens.*, vol. 41, no. 2, pp. 298–302, Feb. 2003.
[12] J. C. Currey, "Geolocation assessment algorithm for CALIPSO using coastline detection, Nat. Aeronaut. Space Admin. (NASA) Langley Res. Center, Hampton, VA, USA, Tech. Rep. NASA/TP-2002-211956, 2002, p. 27.
[13] M. Esplin, K. Robinson, B. Esplin, and D. Scott, "Advanced technology microwave sounder (ATMS) geolocation analysis," in *Proc. Annu. Meet. Amer. Meteorol. Soc.*, 2015, p. 216.
[14] R. Yun, X. Xu, X. Dong, and D.. Zhu, "The processing and simulation of the CFOSAT RFSCAT," in *Proc. Int. Geosci. Remote Sens. Symp.*, 2015, pp. 5332–5335.
[15] M. W. Spencer, C. Wu, and G. Long, "Improved resolution backscatter measurements with the oceanwinds pencil-beam scatterometer," *IEEE Trans. Geosci. Remote Sens.*, vol. 38, no. 1, pp. 89–104, Jan. 2000.
[16] J. Zhu, X. Dong, W. Lin, and D.. Zhu, "A preliminary study of the calibration for the rotating fan-beam scatterometer on CFOSAT," *IEEE J. Sel. Top. Appl. Earth Obs. Remote Sens.*, vol. 8, no. 2, pp. 460–470, Feb. 2015.
[17] J. Liu, Y. Zhang, and X. Dong, "Dechirping compression method for nonlinear frequency modulation waveforms," *IEEE Geosci. Remote Sens. Lett.*, vol. 16, no. 3, pp. 377–381, Mar. 2019.
[18] P. Wessel and W. H. F. Smith, "A global self-consistent, hierarchical, high-resolution shoreline database," *J. Geophys. Res.*, vol. 101, no. B4, pp. 8741–8743, Apr. 1996.
[19] W. P. Byerly and J. C. Storey, "Geolocation visible/infrared imager/radiometer suite algorithm theoretical basis document," *Remo. Sens. Techno. Appl.*, vol. 30, no. 2, pp. 518–526, 2015.
[20] K. Tseng, C. K. Shum, J. Kim, X. Wang, K. Zhu, and X. Cheng, "Integrating landsat imageries and digital elevation models to infer water level change in Hoover Dam," *IEEE J. Sel. Topics Appl. Earth Obs. Remote Sens.*, vol. 9, no. 4, pp. 1696–1709, Apr. 2016.

Kuo Zhang was born in Heilongjiang Province, China, in 1994. He received the B.S. degree in information engineering from Jilin University, ChangChun, China, in 2016. He is currently working toward the Ph.D. degree with the National Space Science Center, Chinese Academy of Sciences, Beijing, China.

He is currently working on the Level 1 data processing of China-France Oceanography Satellite (CFOSAT) Scatterometer.

Xiaolong Dong (Senior Member, IEEE) was born in Shaanxi Province, China, in 1969. He received the B.E. degree in radio technology and the Ph.D. degree in electromagnetic theory and microwave technology from Xi'an Jiaotong University, Xi'an, China, in 1991 and 1996, respectively.

From 1996 to 1999, he was a Postdoctoral Research Fellow and an Associate Professor with the National Space Science Center (NSSC), Chinese Academy of Sciences (CAS), Beijing, China, and was promoted to a Full-Professor, in 1999. From 2001 to 2003, he visited Duke University, Durham, NC, USA. Since November 2003, he has been a Hundred Talents Professor with NSSC, Chinese Academy of Sciences, where he is the Deputy Director-General of the Center and a Professor of the CAS Key Laboratory of Microwave Remote Sensing, Beijing, China. He has been the Principal Investigator of projects for the Scatterometers of Chinese Oceanic Observation Satellites, including the Chinese-French Oceanic Satellite (CFOSAT), and the Haiyang-2 (HY-2) satellite prestudy. He has been the Vice Dean of the School of Astronomy and Space Science, University of Chinese Academy of Sciences (UCAS), Beijing, since 2018 and an Administrative Director of the International Space Science Institute in Beijing (ISSI-BJ) since 2013, respectively. He has authored more than 100 journal articles and conference presentation. His research interests include theory and the techniques of microwave remote sensing, development of advanced microwave sensors, with emphasis on radar scatterometry for atmospheric, oceanic, and land surface applications.

Dr. Dong has been the Chair of the Microwave Sensors Subgroup of the Working Group on Calibration and Validation of the Committee of Earth Observation Satellites, since 2008.

Di Zhu (Member, IEEE) was born in Shaanxi, China, in 1978. He received the B.S. degree in communication engineering and the M.S. degree in electromagnetic and microwave engineering from Xi'an Jiaotong University, Xi'an, China, in 2001 and 2004, respectively, and the Ph.D. degree in computer application technology from the Chinese Academy of Sciences, Beijing, China, in 2008.

He is with the National Space Science Center, Chinese Academy of Sciences. He has been the Deputy Chief Designer of the China-France Oceanography Satellite (CFOSAT) Scatterometer. His research interests include spaceborne and airborne remote sensing payload design and signal processing.

Risheng Yun (Member, IEEE) was born in Inner Mongolia, China, in 1974. He received the B.Sc. degree in computational mathematics from Lanzhou University, Lanzhou, China, in 1995, the M.Sc. degree in engineering from Northwestern Polytechnical University, Xi'an, China, in 2001, and the Ph.D. degree in engineering from the Institute of Electronics, Chinese Academy of Sciences, Beijing, China, in 2003.

From 2011 to 2012, he was a Visiting Scientist with the Royal Netherlands Meteorological Institute, De Bilt, The Netherlands, where he is working on the Numerical Weather Prediction (NWP) Ocean Calibration for scatterometers. He is currently a Research Staff with the National Space Science Center, Chinese Academy of Sciences, where he is working on scatterometer data processing.